Biomed Microdevices (2017) 19: 102
https://doi.org/10.1007/s10544-017-0245-5

Engineered bone scaffolds with Dielectrophoresis-based patterning using 3D printing

Zhijie Huan[1,2,3] · Henry K. Chu[4] · Hongbo Liu[1] · Jie Yang[2] · Dong Sun[1]

Published online: 13 November 2017

Abstract Patterning of cells into a specific pattern is an important procedure in tissue engineering to facilitate tissue culture and ingrowth. In this paper, a new type of 3D–printed scaffold utilizing dielectrophoresis (DEP) for active cell seeding and patterning was proposed. This scaffold adopted a concentric-ring design that is similar to native bone tissues. The scaffold was fabricated with a commercial three-dimensional (3D) printer. Polylactic Acid (PLA) was selected as the material for the printer and the fabricated scaffold was coated with gold to enhance the conductivity for DEP manipulation. Simulation from COMSOL confirmed that non-uniform electric fields were successfully generated under a voltage input. The properties of the scaffold were first characterized through a series of experiments. Then, preosteoblast MC3T3-E1 cells were seeded onto the coated scaffold and multiple cellular rings were observed under the microscope. The biocompatibility of the material was also examined and mineralized bone nodules were detected using Alizarin Red S Staining after 28 days of culture. The proposed scaffold design can enable formation of multiple ring patterns via DEP and the properties of the scaffold are suitable for bone tissue culture. This new type of 3D–printed scaffold with cell seeding mechanism offers a new and rapid approach for fabricating engineered scaffolds that can arrange cells into different patterns for various tissue engineering applications.

Keywords 3D printing · Bone scaffold · Cell patterning · Dielectrophoresis · Polylactic acid

✉ Dong Sun
medsun@cityu.edu.hk

[1] Department of Mechanical and Biomedical Engineering, City University of Hong Kong, Kowloon, Hong Kong

[2] Department of Precision Machinery and Instrumentation, University of Science and Technology of China, Hefei, Anhui, China

[3] School of Electrical Engineering and Automation, XiaMen University of Technology, Xiamen, China

[4] Department of Mechanical Engineering, The Hong Kong Polytechnic University, Kowloon, Hong Kong

1 Introduction

Additive manufacturing, often known as 3D printing, has opened up new opportunities for the manufacture of customized products. In the field of medical science, 3D printing allows patient-specific surgical implants, prostheses, and scaffolds to be fabricated rapidly with low cost, offering greater convenience and flexibility for surgeons and patients. When choosing the proper 3D printing technology, material selection is very important because these implants or scaffolds have to be placed inside the patient body. Nowadays, common polymeric materials that can be used for 3D printing include Polylactic Acid (PLA) (Pavia et al. 2012; Guarino et al. 2008; Liu et al. 2015), Acrylonitrile Butadiene Styrene (ABS) (McCullough and Yadavalli 2013), Polycaprolactone (PCL) (Williams et al. 2005) and PolyEthylene Terephthalate (PET) (Ma et al. 2005). In particular, PLA has received extensive attention because of its high biocompatibility and biodegradability. PLA is extracted from Lactic acid, which can be easily produced through the fermentation of starchy materials or sugar. When PLA is immersed in the body fluid, it can be hydrolyzed and gradually metabolized and bio-absorbed by cells (Tokiwa and Calabia 2006). In addition, PLA possesses excellent mechanical properties, which allows direct 3D printing of complicated structures without the need of any supporting material. Due to its properties, PLA has been

approved by the Food and Drug Association (FDA) for various biomedical applications (Uhrich et al. 1999).

Tissue engineering is the research of utilizing cells and engineered scaffolds for the development of functional tissues. Since biological cells are very sensitive to the culture environment, in additional to the material, the scaffold design and its structural parameters should also be tailored in order to provide an optimal environment for tissue culture. In general, scaffolds fabricated with conventional techniques often lack the capability to precisely control intrinsic properties such as pore size, morphology, and interconnectivity. On the contrary, 3D printing can overcome these limitations. For instance, Cox et al. (2015) printed a 3D cylindrical scaffold with interconnected pores for bone applications. Almeida et al. (2014) examined the orthogonal and diagonal pore networks by adjusting the angle of material deposition between layers. To characterize the cellular responses, Sobral et al. (2011) proposed a scaffold design with gradual pore sizes and the results indicated an increase in the seeding efficiency over homogeneous scaffold designs. Yeo et al. (2012) examined the pore network with different offset values and concluded that having offsets can increase the cell-seeding efficiency and water-uptake ability.

Bone fracture caused by disease or injury is a serious problem to the patients. On many occasions, suitable autografts or allografts may not be available and engineered bone grafts through the tissue engineering approach could provide a promising alternative to these grafts. For culturing large scale scaffolds, achieving a high initial cell density is a crucial step towards the quality of the developed tissues. To date, majority of the studies, including the aforementioned studies, mainly employed a passive cell seeding mechanism, which relies on the medium to penetrate through the scaffold for cell attachment. In addition, cells adhered to the inner parts of the scaffold could gradually sink to the bottom due to the gravity. As pointed out by Wust et al. (2011), one drawback in current cell seeding techniques is that cells are mostly randomly distributed on the scaffold, but ideally, cells should be specifically arranged to facilitate tissue culture and ingrowth. Hence, an active cell seeding mechanism that can automatically pattern and hold cells in three-dimensional space can further advance the research on tissue engineering. To date, there are a number of non-invasive techniques that can be used to manipulate cells. For instance, optical tweezers utilize highly focused laser beams (Chowdhury et al. 2014; Yan and Sun 2015; Cheah et al. 2014) to trap and organize cells in a desired pattern. However, this method has relatively low throughput for cell manipulation and potential laser-induced photodamage of cells (Mirsaidov et al. 2008). Magnetic field has also been investigated for batch manipulation of cells through force induced on magnetic nanoparticles attached to cell surfaces. To minimize the influence on cells, the magnetic nanoparticles should be biocompatibility and non-toxicity for tissue engineering (Ito et al. 2005, Miltenyi et al. 1990). Unlike the above methods, Dielectrophoresis (DEP) approach aims to manipulate dielectric particles through non-uniform electric fields (Gagnon et al. 2010; Ho et al. 2013). Since cells are dielectric in nature, additional treatments such as attaching magnetic nanoparticles to the cells are not necessary.

In our previous study, a scaffold for active cell seeding, made of stainless steel, was proposed for the regeneration of bone tissues (Huan et al. 2016). Honey-comb cellular patterns were formed on different layers of the scaffold through the dielectrophoresis mechanism. In the current paper, we present a new method to integrate active cell seeding mechanism on 3D printed scaffolds. This scaffold adopted a simpler design so that 3D dielectrophoresis can be incorporated through a single layer of scaffold. Based on the application, scaffolds with concentric-ring design were first fabricated using commercial 3D printer so as to mimic the native bone tissues. PLA was selected as the printing material because of its high biocompatibility and corrosion resistance. To enable cell seeding via dielectrophoresis, the scaffold was coated with a thin layer of gold to enhance electrical conductivity. Experiments were conducted to examine the performance of cell seeding via the proposed method. The effects of dielectrophoresis as well as the material properties on the cell behaviors were also examined and characterized experimentally.

2 Materials and methods

2.1 Scaffold design

Over years, a number of PLA-based scaffolds have been reported for tissue engineering applications. For instance, Salerno et al. (2015) examined the scaffold with mean pores ranging from 170 to 440 μm through porogen leaching, and the results indicated that the cell viability between scaffolds with smaller and larger mean pores are comparable after 7 days of culture. Rosenzweig et al. (2015) and Almeida et al. (2014) examined 3D–pinted orthogonal scaffolds with pore size of 700 μm, and 1000 mm, respectively. Both results showed that cells on the scaffolds display high viability and well adhesion. As summarized in (Murphy et al. 2010), scaffolds with pore sizes ranging from 20 to 1500 μm had been used for bone tissue engineering applications. In this work, a multi-layer scaffold with pore sizes of 500 μm was considered for the experiments. According to the literature (Bao et al. 2013; Rho et al. 1998; Weiner et al. 1999; Olszta et al. 2007), Osteon is the main structural unit of a bone, which consists of concentric layers of lamellas, as shown in Fig. 1a. To mimic the structure of a native bone, the scaffold design adopts a similar concentric-ring structure, as shown in Fig. 1b, c. Since culturing large-scale scaffolds can increase the risk of cell death due to limited oxygen and nutrient diffusion (Amini

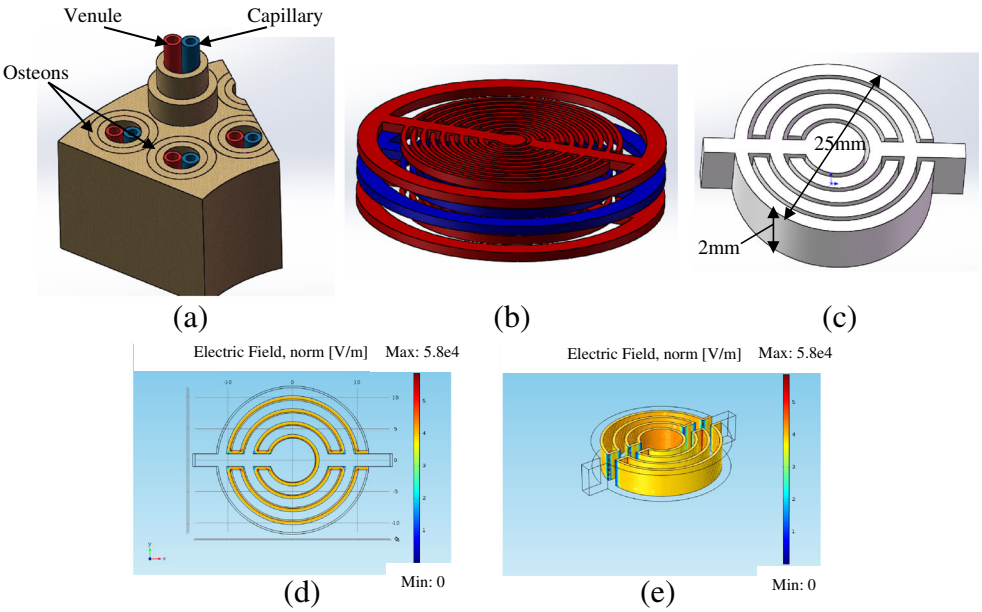

Fig. 1 Scaffold design. **a** Schematic diagram of a bone. **b** Multi-layer scaffold design. **c** Design of individual scaffold layer. **d** and **e** Electric field simulation of the scaffold under a voltage input in 2D and 3D

et al. 2012), the proposed design can allow the cells to seed in individual layers for cell proliferation and subsequent culture. Afterward, cell-seeded layers will be stack to construct the multi-layer scaffold. Each layer of the scaffold, with an outer diameter of 25 mm, has multiple concentric rings. Each ring has a width of 500 μm and a thickness of 2 mm. There is a gap of 500 μm between the rings, which will provide a space for cell attachment and allow nutrients to transport through the scaffold. As discussed previously, cells seeded on the scaffold, especially the vertical side wall, through the conventional method could easily be sunk to the bottom due to gravity. To avoid that, non-contact and non-invasive techniques could be incorporated for cell manipulation (Ho et al. 2013; Lin et al. 2006). In this design, dielectrophoresis is incorporated to manipulate cells (Zhang et al. 2008; Gasperis et al. 1999; Zou et al., 2006), forming 3D concentric cellular ring patterns during the cell seeding process. The working principle of DEP is to utilize non-uniform electric fields to induce forces on polarizable particles. The equation describing the DEP force is given by Pohl (1978):

$$F_{DEP} = 2\pi r^3 \varepsilon_m \mathrm{Re}[K(\omega)]\nabla\left|\vec{E}\right|^2$$

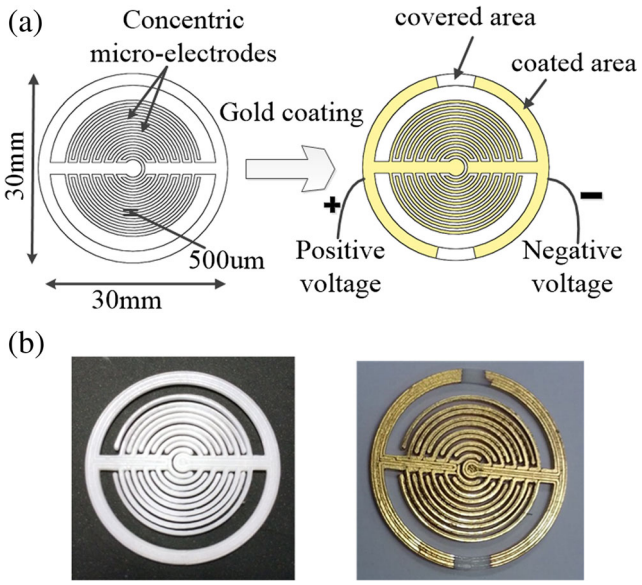

Fig. 2 The electrode-integrated scaffold design. **a** Connecting wires. **b** Images of the coated and uncoated scaffolds

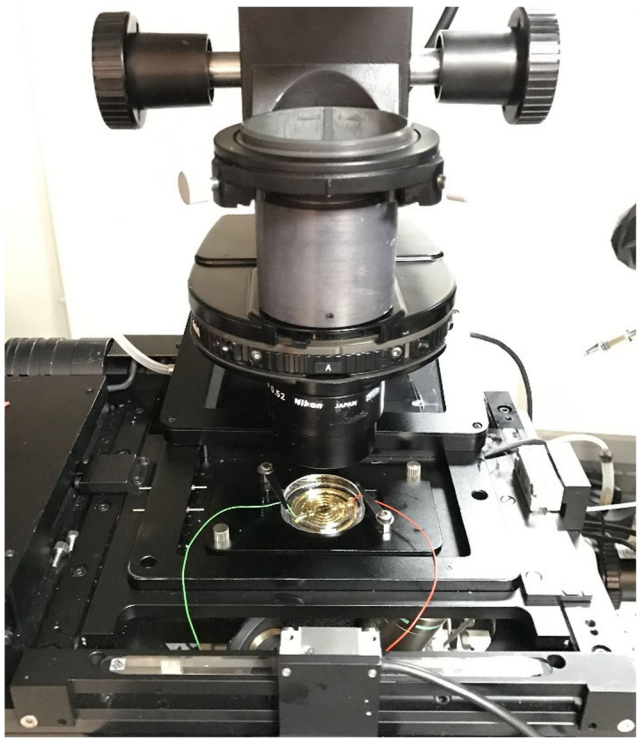

Fig. 3 Experimental setup for DEP cell patterning onto the scaffold

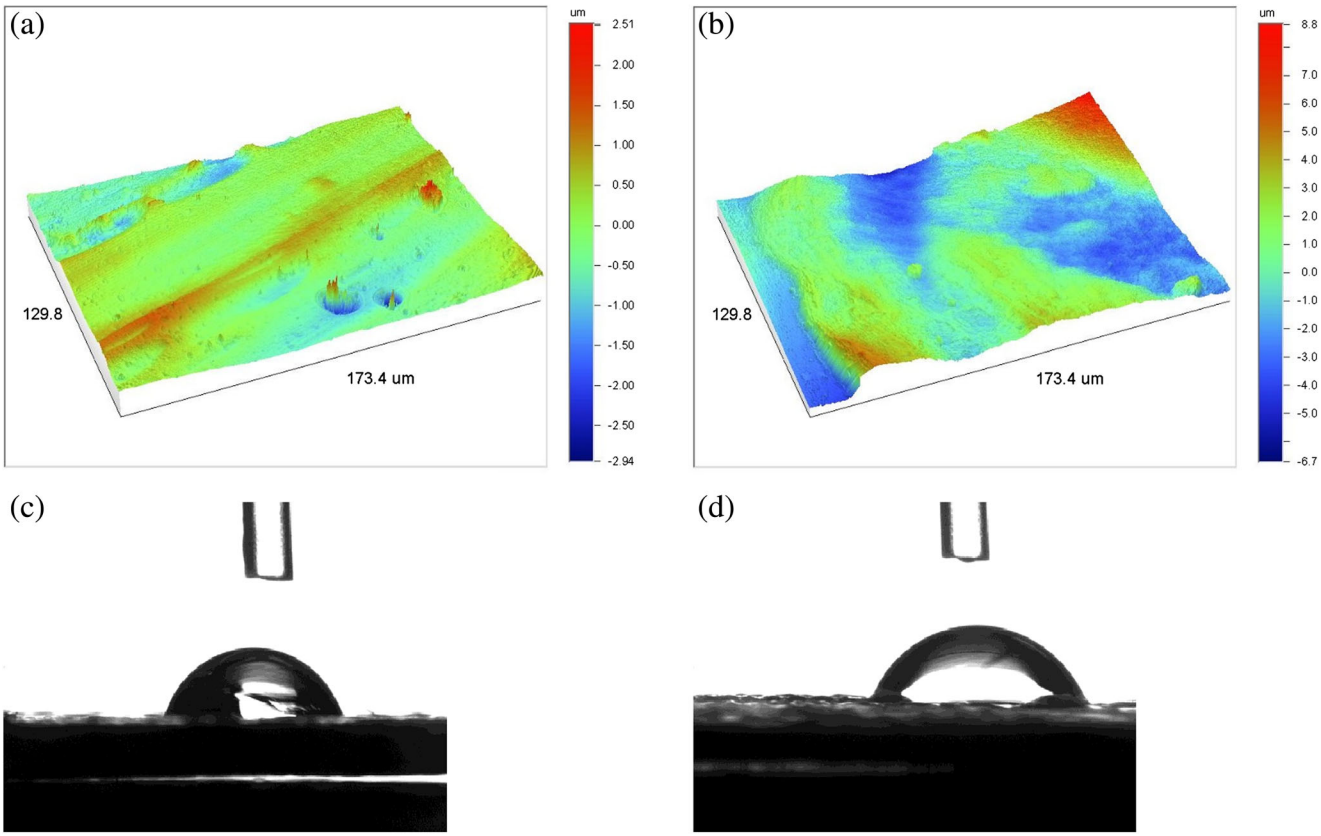

Fig. 4 Surface roughness and contact angle. **a** 3D image showing the surface roughness of the coated scaffold. **b** 3D image showing the surface roughness of the uncoated scaffold. **c** Contact angle measurement on the coated scaffold. **d** Contact angle measurement on the uncoated scaffold

where r is the cell radius, ε_m is the permittivity of the medium, $\nabla\left|\overrightarrow{E}\right|^2$ is the gradient of the square of the effective AC electric field, Re[$K(\omega)$] is the real part of the Clausius-Mossotti (CM) factor. The sign of the CM factor determines the direction of the DEP force on the cell, which is based on the relative polarizability of the cell and the medium. A positive DEP force will direct the cells toward the high field regions while a negative DEP force will repel the cells to the low field regions.

In this work, a positive DEP force is utilized for cell patterning. The use of DEP for patterning cells onto the scaffold has also been reported in our earlier studies (Huan et al. 2016; Chu et al. 2015). A finite element software, COMSOL, was used to simulate the electric field distribution as generated from the current scaffold design. Simulation results as shown in Fig. 1d, e confirm that high electric field regions can be achieved in the gaps between the concentric rings, thereby enabling concentric-ring cellular patterns to be constructed.

Table 1 Resistivity of different coating thickness

Coating time(s)	Thickness (nm)	Resistance (Mean value) (Ω/cm)	Standard deviation (Ω/cm)
60	17.2	33.57	3.9
120	34.8	10.53	0.41
300	88.8	4.33	0.47
600	174.8	1.13	0.17

2.2 Scaffold fabrication

A commercial 3D printer (M3D), employing the fused deposition modeling (FDM) technology, was used to fabricate the scaffold. Nozzle-deposition based 3D printing has shown great versatility and is capable of fabricating well-defined 3D structures with high precision and repeatability. The nozzle tip of the printer has a diameter of 350 μm and the minimum layer thickness is 50 μm. Standard PLA filaments with 1.75 mm size is selected as the structural material for printing the scaffold and materials are deposited layers by layers to construct the 3D structure. The geometry of the scaffold was first modeled using Solidworks and then converted to a STL file for printing.

Similar to many polymeric materials, PLA is not electrically conductive. Polymeric materials can become conductive by mixing with conductive fillers like metal

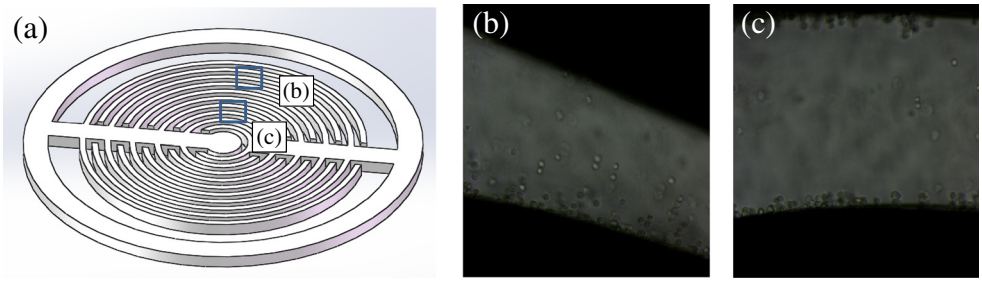

Fig. 5 Microscope image of MC3T3-E1 cells patterned at different locations of the scaffold. **a** 3D schematic. **b** Outer ring. **c** Inner ring

particles or through doping. Nevertheless, their electrical conductivities may not be as high as metals. In this work, a thin layer of gold was coated onto the fabricated structure using the sputtering system (Quorum Q150TS), as shown in Fig. 2. Gold is selected as the target material for sputtering because gold is known to be biologically inert, which is safe to be implanted in human body. The coating method can achieve high electrical conductivity while minimizing the use of the material. Prior to the experiment, the scaffold was immersed in a 70% ethanol for sterilization and then coated with poly-L-lysine (Sigma Aldrich) to enhance the surface affinity for cell attachment.

2.3 Cell preparation

In this work, preosteoblast MC3T3-E1 cells derived from mouse calvaria were selected as samples for cell patterning with the proposed scaffold. Preosteoblast cells can be differentiated into osteoblast cells, which are responsible for formation of new bones. MC3T3-E1 cells were first proliferated in a 35 mm Petri dish using Dulbecco's modified Eagle's medium (DMEM) containing 10% (*v*/v) heat-inactivated fetal bovine serum (FBS) and 1% (v/v) penicillin–streptomycin. The Petri dish was incubated at 37 °C with a gas mixture of 95% air and 5% CO_2. The culture medium was changed every two days until confluency.

To harvest cells from the Petri dish for the experiment, the cells were washed with phosphate-buffered saline (PBS) and then trypsinized using a 0.25% trypsin–EDTA solution. The cells were then detached from the Petri dish and transferred to a centrifuge tube to obtain the cell pellet. The cell pellet was aspirated with a low-conductivity buffer medium containing 8.5% sucrose, 0.3% dextrose, and 20 mg/L $CaCl_2$ (Puttaswamy et al. 2010) so that the cells could be more polarizable than the buffer medium, inducing a strong p-DEP effect. This buffer medium was tested previously and over 90% of cell viability could be maintained. The concentration of the cell droplets used for the experiments was approximately 5×10^4 cells/mL.

2.4 DEP cell patterning

DEP cell patterning was performed by connecting an AC function generator, GW Instek, GFG8255A, to the scaffold as shown in Fig. 3. The scaffold was mounted on a 35 mm petri dish and the formation of cellular patterns through DEP was observed using an inverted microscope system, Nikon Eclipse Ti. A droplet of the prepared cell medium was pipetted to the scaffold layer to fill the gaps in between the rings. Afterward, a sinusoidal voltage was applied to two ends of the layer to induce DEP force on the cells. As discussed in our previous study (Huan et al. 2016), a frequency ranged between 100 kHz and 1 MHz could yield the maximum positive DEP force for cell manipulation. A higher voltage input as well as a longer DEP patterning time could decrease the cell viability rate. In this experiment, the voltage input was set to 10 V at a frequency of 1 MHz, and the patterning time was kept in 5 min to minimize cell lysis.

After DEP patterning, regular culture medium was added to the petri dish through a syringe pump (KD Scientific) and the scaffold was incubated for 7 days. The cell morphology and the pattern on the scaffold were

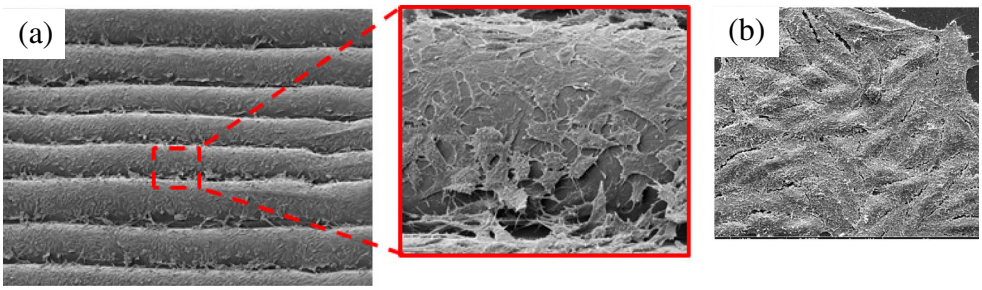

Fig. 6 SEM image of the attached cells. **a** Cells on the vertical sidewall of the scaffold at 100 × and 800 × magnification. **b** Cells on the Petri dish (control) at 800 × magnification

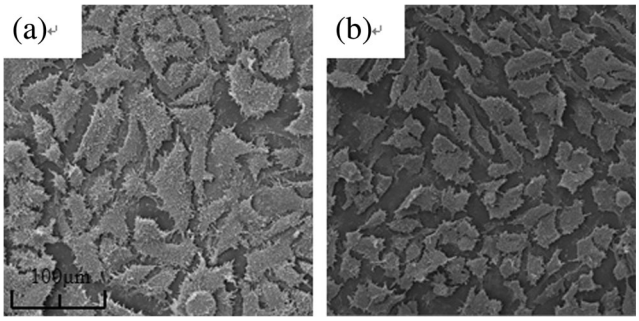

Fig. 7 Cell morphology after 4d culture. **a** SEM image on uncoated PLA. **b** SEM image on gold coated PLA

inspected using Scanning Electron Microscope (SEM). Cells were fixed with 4% paraformaldehyde (PFA), dried with a Critical Point Dryer (Leica EM CPD300), and then gold-coated for SEM study. Micrographs were taken at an accelerating voltage of approximately 20 keV at different magnifications.

2.5 Bone nodule formation

The formation of the mineralized bone nodules from the selected cell type was assayed using Alizarin Red S (Sigma Aldrich). This stain can be used to identify calcium (mineral) on the scaffold with red color. A 24-well culture plate was used for the study and cells containing droplets were pipetted to each well to prepare four sets of specimens. In the first set, cells were incubated with DMEM and used as the control. To induce cell differentiation and nodule formation, the culture medium in the second set was changed to alpha-MEM containing 10 mmol/L β-glycerophosphate and 50 μg/mL ascorbic acid (Sprague et al. 1993, Bushinsky 1994). In the third and fourth sets, miniature scaffolds were placed in each well and cultured with DMEM and alpha-MEM, respectively. After 7 days, 14 days, 21 days and 28 days of culture, specimens from each group were stained using Alizarin Red S to assess the amount of calcium deposition by cells (Balint et al. 2001).

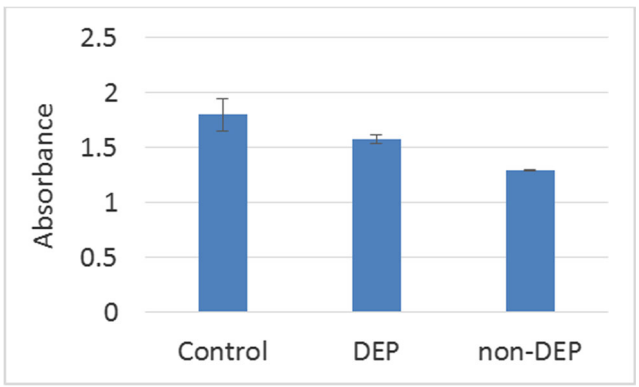

Fig. 8 MTT assay of MC3T3-E1 cells on different specimens

3 Results and discussion

3.1 Scaffold characterization

The properties of the scaffold were evaluated on four aspects: the mechanical strength, the porosity, the durability, and the wettability. An ideal scaffold should possess a Young's modulus that is comparable to a typical bone of around 20GPa (Polo-Corrales et al. 2014). The modulus of the scaffold was examined using a micro hardness tester (Fischerscope) and the indentation moduli measured at four random test points were recorded. The average moduli for the uncoated and the coated sides of the scaffold are approximately 4.79 ± 0.16 GPa and 4.22 ± 0.14 GPa, respectively, which are close to the modulus of pure PLA material (Rosenzweig et al. 2015). The coated side was found to have a lower modulus than the uncoated side, which could be due to the error in obtaining an accurate contact area for hard coating film on a soft substrate (Chen et al. 2005).

The porosity of the proposed scaffold was evaluated using the equation (Serra et al. 2013):

$$\%Vol_{theoretical} = \left(\frac{V_a - V_t}{V_a}\right) \times 100\%$$

where V_a is the apparent volume (area x height), and V_t is the true volume. Based on the scaffold design, the theoretical volume percentage is calculated to be 34%. As reported by Bose et al. (2013), the cancellous bone has a porosity of 30% to 90% and the porosity of bone scaffolds adopted by other groups mainly fall in this range.

The durability of the coated scaffold was also examined and the scaffold was immersed in medium and incubated for 7 days. The electrical conductivity of the scaffold was measured again after 7 days and no significant difference was found. Also, the weight of the scaffold was monitored and the weight of the scaffold changes from 0.775 g to 0.756 g, dropping less than 2.5% of its weight after 7 days of culture.

The influence of the gold coating on the wettability of the scaffold was characterized through two tests and the results were shown in Fig. 4. In the first test, the contact angle of the scaffold surface was measured with an in-house system. After coating, the contact angle averaged from five trials changed from 60 degrees to 63 degrees, resulting in more hydrophobic surface to hinder cell attachment. The results obtained from the Surface Profiler (Veeco), also indicated that, after coating, the scaffold has a more uniform surface, with the roughness decreases from 1593 μm to 414 μm, providing a less favorable surface for cell attachment.

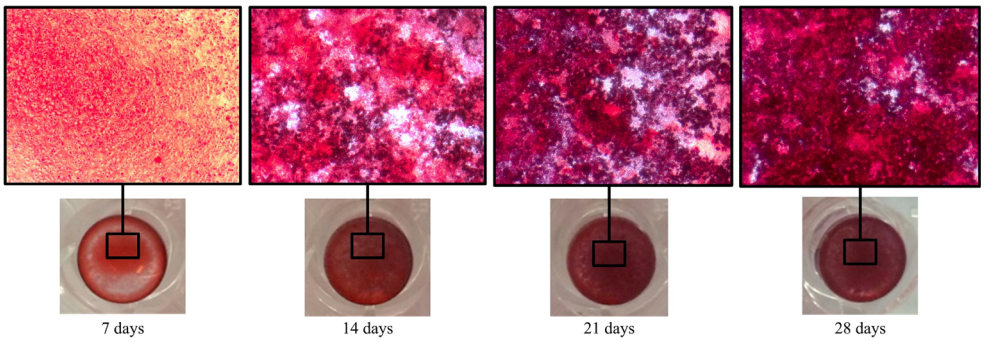

Fig. 9 Alizarin Red S stains of the calcium distribution after each experimental period: 7 days, 14 days, 21 days, and 28 days.

3.2 DEP patterning

To facilitate DEP cell patterning, it is important to ensure the scaffold, especially the inner surface, to be conductive through the coating method. When a voltage is applied to the scaffold, non-uniform electric fields can thus be generated so that suspending cells are polarized and manipulated toward the scaffold body. The duration of the coating is one of the main parameters controlling the coating thickness, thereby affecting the conductivity and the uniformity of the coated material. Prior to the experiment, a multimeter was used to check the resistance value of the material. Four different coating durations, 60s, 120 s, 300 s and 600 s, were considered in this work. For each coated scaffold, the resistance values at three different locations were measured and the results are summarized in Table 1. From the results, it is noted that all four durations can successfully provide a sufficient coating to allow the scaffold to be conductive. The average resistance value changes from $33.57 \pm 3.9\ \Omega$/cm to $1.13 \pm 0.17\ \Omega$/cm as the coating time increases. Nevertheless, the standard deviation for a coating duration of 60s is much higher than the others, indicating a high variability with this coating duration. This error could be due to uneven coating on the specimen with rough surface. A longer duration time can improve the conductivity of the material (Wei et al. 2006), but also consume more target material. In our study, a coating thickness of 35 nm (120 s) was eventually selected for the experiments.

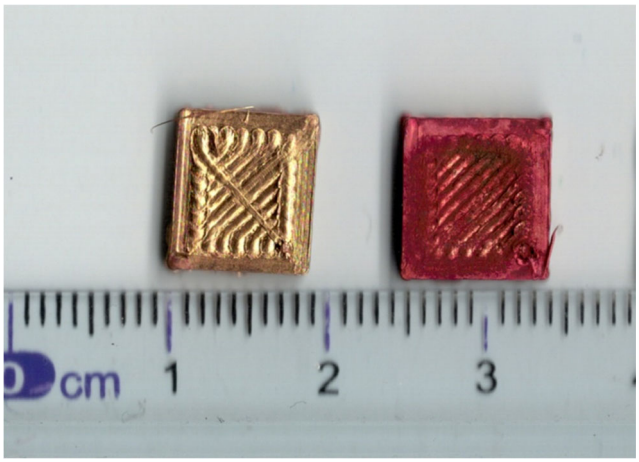

Fig. 10 Alizarin Res S stain of the calcium deposition, *left:* gold coated PLA scaffold cultured with DMEM; right: gold coated PLA scaffold cultured with alpha-MEM

Afterward, 0.5 mL of cell droplets were pipetted to the scaffold and the results show that cells were immediately polarized and adhered to the scaffold, forming multiple cellular ring patterns as shown in Fig. 5b, c. The cellular patterns found at the inner and outer rings confirm that DEP force was successfully generated throughout the entire scaffold for cell patterning. The density of the cellular patterns at the inner ring and the outer ring are comparable. This can be explained from the simulation results in Fig. 1d, e. The strength of the DEP force is dependent on the electric field, where the field strength and distribution are similar at the two regions. Experimental results also confirm that the formed cellular patterns can be retained when fresh medium was added to the petri dish using a syringe pump.

The seeded scaffold was then cultured for 7 days and inspected using SEM. The scaffold was dehydrated and coated with gold as described in the previous section. SEM images in Fig. 6 show that the PLA scaffold material after gold coating can provide a good surface for cell attachment. Cells attached on the surface via DEP continued to proliferate, and expanded to different layers of the scaffold with a good surface coverage after 7 days. The cell morphology on the scaffold after 7 days of culture is comparable to the one cultured on Petri dish, indicating that the effect of DEP on the cell behavior is negligible.

The metabolic activity of the cells on the DEP-patterned scaffold was assayed using MTT cell proliferation assay kit. Cells were seeded onto two scaffolds with and without voltage supply, respectively, and cells were also seeded on a Petri dish as the control. After 7 days of culture, the three specimens were incubated with MTT reagent for 4 h, which yellow tetrazole in the reagent was cleaved to purple formazan by viable cells. The formazan crystals dissolved in the solubilization solution were then quantified using microplate reader at 570 nm. The absorbance values from the three specimens were measured and the results are shown in Fig. 7. From the results, the value for the scaffold with DEP patterning is

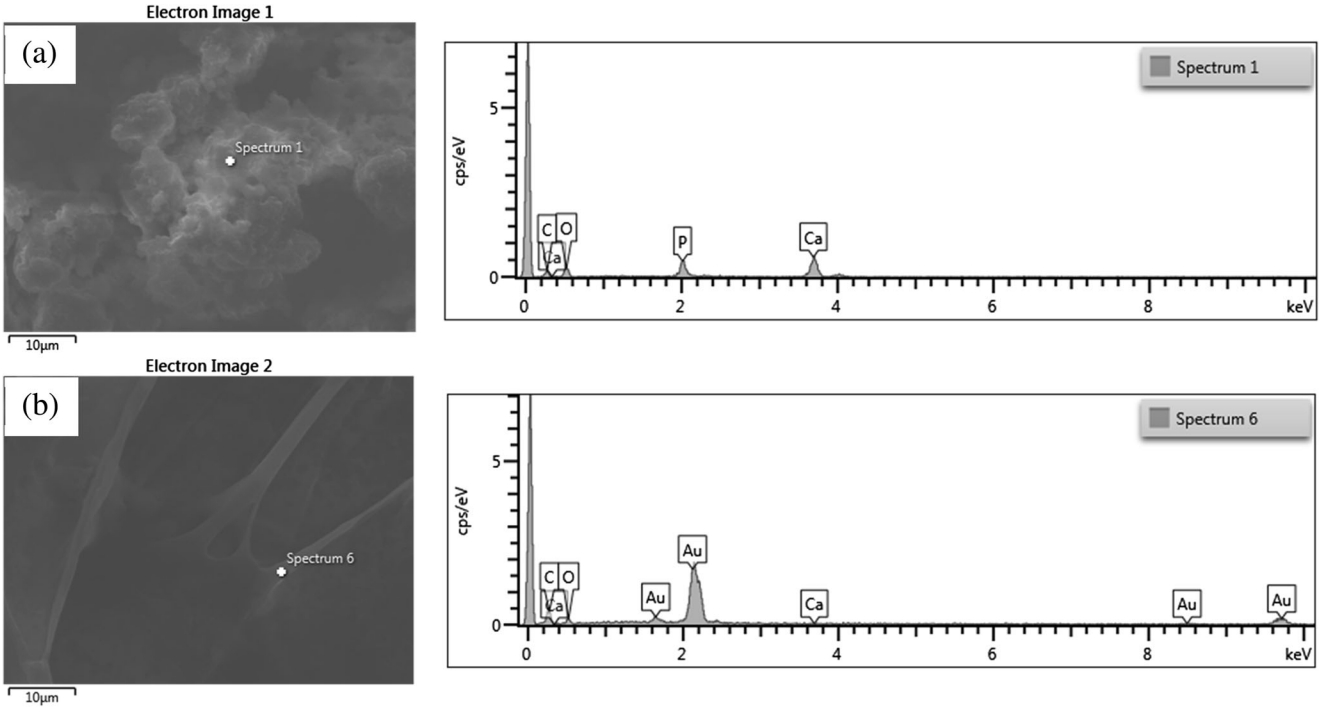

Fig. 11 EDX results showing the composition of the scaffold cultured in (a) Alpha-MEM and (b) DMEM

higher than the non-DEP scaffold, indicating the presence of more cells on the scaffold. Among the three specimens, the control has highest number and it can be explained as the 2D surface can provide a more planar and optimal environment for cell proliferation and culture.

3.3 Biocompatibility of the material

To further examine whether or not the gold-coated scaffold material has any influence on the cell behavior, cells were seeded and culture on PLA and gold-coated PLA substrates, respectively. After 4 days of culture, no significant difference on the cell morphology was observed from the two substrates, as shown in Fig. 8. However, PLA substrate can achieve a higher cell density, which may due to the surface roughness. The uncoated surface has a less uniform surface, which promotes cell attachment (Hao et al. 2004).

3.4 Bone nodule formation

To evaluate the formation of bone nodule, specimens on the 24-well culture plate were characterized. Alizarin Red S stain was used to assess the calcium deposition by cells, which were stained in red color. From the first control group, scattered red dots were observed in the well but no significant increase in the amount of calcium deposition (red dots) was found after 28 days of culture. For the second group of cells cultured with alpha-MEM, the formation of bone nodule was more obvious. As shown in Fig. 9, a cluster of red dots were observed on the well after 7 days. After 14 days, the entire well was almost covered by red dots. After 21 and 28 days, the wells were covered by red dots, indicating a positive result on the culture protocol and the assay for bone nodule formation. For the third group, the scaffold did not turn red after 28 days of culture, as illustrated in Fig. 10. For the scaffold cultured with alpha-MEM, the scaffold was turned to deep red, indicating the presence of a high amount of calcium throughout the scaffold material, as illustrated in Fig. 11. The result also confirms that the material is suitable for cell culture and bone nodule formation. To further examine the mineral deposition, the two cultured scaffolds were characterized using Energy-dispersive X-ray spectroscopy (EDX) to detect the material composition. From the results, calcium signals can be detected from the scaffold cultured with alpha-MEM, while very low calcium signals can be detected from the scaffold cultured with DMEM, as shown in Fig. 11.

4 Conclusion

This paper presented a new type of scaffold that can be fabricated with 3D printing technology. Biocompatible PLA material was selected as the printing material and the electrical conductivity of the printed scaffold was enhanced through the process of gold coating. This scaffold adopted a concentric ring design, and its geometric

properties can facilitate rapid formation of multiple cellular ring patterns via dielectrophoresis. Experiments were conducted to confirm that the scaffold material and its properties are suitable for cell culture. The conductivity and the durability of the coating on the scaffold were also examined and confirmed through experiments. Afterward, MC3T3-E1 cells were seeded onto the scaffold and multiple cellular ring patterns could be observed at different parts of the scaffold. Images from SEM show that the patterned cells remained adhered on the scaffold surface and continued to proliferate. Four sets of specimens were prepared to show that the scaffold and the culture protocol are appropriate to enable bone nodule formation after 28 days of culture. Hence, this 3D–printed engineered scaffold can be combined with dielectrophoresis to enable rapid patterning of cellular patterns for bone tissue culture.

Acknowledgments This work is supported by grants from the Research Grant Council of the Hong Kong Administrative Region, China, with (Reference No. CityU 11267916 and N_CityU 102/15).

References

C.R. Almeida, T. Serra, M.I. Oliveira, J.A. Planell, M.A. Barbosa, M. Navarro, Acta Biomater. **10**, 613 (2014)
A.R. Amini, C.T. Laurencin, S.P. Nukavarapu, Crit. Rev. Biomed. Eng. **40**, 363 (2012)
E. Balint, P. Szabo, C.F. Marshall, S.M. Sprague, Bone **28**, 21 (2001)
C. L. M. Bao, E. Y. Teo, M. S. Chong, Y. Liu, M. Choolani, J. K. Chan, Regenerative medicine and tissue engineering. Intech. (2013). https://doi.org/10.5772/55916
S. Bose, S. Vahabzadeh, A. Bandyopadhyay, Mater. Today **16**, 496 (2013)
D.A. Bushinsky, Kidney Int. **46**, 1199 (1994)
C.C. Cheah, X. Li, X. Yan, D. Sun, IEEE Trans. Robot. **30**, 68 (2014)
S. Chen, L. Liu, T. Wang, Surf. Coat. Technol. **191**, 25 (2005)
S. Chowdhury, A. Thakur, P. Svec, C. Wang, W. Losert, S.K. Gupta, IEEE Trans. Autom. Sci. Eng. **11**, 338 (2014)
H.K. Chu, Z. Huan, J.K. Mills, J. Yang, D. Sun, Lab Chip **15**, 920 (2015)
S.C. Cox, J.A. Thornby, G.J. Gibbons, M.A. Williams, K.K. Mallick, Mater. Sci. Eng. C **47**, 237 (2015)
Z. Gagnon, M. Jill, H.C. Chang, Lab Chip **10**, 718 (2010)
G.D. Gasperis, J. Yang, F.F. Becker, P.R.C. Gascoyne, X.B. Wang, Biomed. Microdevices **2**, 41 (1999)
V. Guarino, F. Causa, P. Taddei, M. di Foggia, G. Ciapetti, D. Martini, C. Fagnano, N. Baldini, L. Ambrosio, Biomaterials **29**, 3662 (2008)
L. Hao, J. Lawrence, Y.F. Phua, K.S. Chian, G.C. Lim, H.Y. Zheng, J. Biomed. Mater. Res. B Appl. Biomater. **7**, 148 (2004)
C.T. Ho, R.Z. Lin, R.J. Chen, C.K. Chin, S.E. Gong, H.Y. Chang, H.L. Peng, L. Hsu, T.R. Yew, S.F. Chang, C.H. Liu, Lab Chip **13**, 3578 (2013)
Z. Huan, H.K. Chu, J. Yang, D. Sun, IEEE Trans. Biomed. Eng. **64**, 755 (2016)
A. Ito, M. Shinkai, H. Honda, T. Kobayashi, J. Biosci. Bioeng **100**, 1 (2005)
R. Lin, C. Ho, C. Liu, H. Chang, Biotechnol. J. **1**, 949 (2006)
H. Liu, R. Wang, H.K. Chu, D. Sun, J. Biomed. Mater. Res. A **103**, 2966 (2015)
Z. Ma, M. Kotaki, T. Yong, W. He, S. Ramakrishna, Biomaterials **26**, 2527 (2005)
E.J. McCullough, V.K. Yadavalli, J. Mater. Process. Technol. **213**, 947 (2013)
S. Miltenyi, W. Muller, W. Weichel, A. Radbruch, Cytometry **11**, 231 (1990)
U. Mirsaidov, W. Timp, K. Timp, M. Mir, P. Matsudaira, G. Timp, Phys. Rev. E **78**, 021910 (2008)
C.M. Murphy, M.G. Haugh, F.J. O'Brien, Biomaterials **31**, 461 (2010)
M.J. Olszta, X. Cheng, S.S. Jee, R. Kumar, Y.Y. Kim, M.J. Kaufman, E.P. Douglas, L.B. Gower, Mater. Sci. Eng. R. Rep. **58**, 77 (2007)
F.C. Pavia, S. Rigogliuso, V.L. Carrubba, G.A. Mannella, G. Ghersi, V. Brucato, Chem. Eng. Trans. **27**, 107 (2012)
H.A. Pohl, *Dielctrophoresis* (Cambridge University Press, Cambridge, 1978)
L. Polo-Corrales, M. Latorreesteves, J.E. Ramirezvick, J. Nanosci. Nanotechnol. **14**, 15 (2014)
S.V. Puttaswamy, S. Sivashankar, R.J. Chen, C.K. Chin, H.Y. Chang, C.H. Liu, Biotechnol. J. **5**, 1005 (2010)
J.Y. Rho, L. Kuhnspearing, P. Zioupos, Med. Eng. Phys. **20**, 92 (1998)
D.H. Rosenzweig, E. Carelli, T. Steffen, P. Jarzem, L. Haglund, Int. J. Mol. Sci. **16**, 15118 (2015)
A. Salerno, M. Fernández-Gutiérrez, J.S.R.D. Barrio, C. Domingo, J. Supercrit. Fluids **97**, 238 (2015)
T. Serra, J.A. Planell, M. Navarro, Acta Biomater. **9**, 5521 (2013)
J.M. Sobral, S.G. Caridade, R.A. Sousa, J.F. Mano, R.L. Reis, Acta Biomater. **7**, 1009 (2011)
S.M. Sprague, N.S. Krieger, D.A. Bushinsky, Am. J. Physiol. **264**, 882 (1993)
Y. Tokiwa, B.P. Calabia, Appl. Microbiol. Biotechnol. **72**, 244 (2006)
K.E. Uhrich, S.M. Cannizzaro, R.S. Langer, K.M. Shakesheff, Chem. Rev. **99**, 3181 (1999)
Q.F. Wei, H. Ye, D.Y. Hou, H.B. Wang, W.D. Gao, J. Appl. Polym. Sci. **99**, 2384 (2006)
S. Weiner, W. Traub, H.D. Wagner, J. Struct. Biol. **126**, 241 (1999)
J.M. Williams, A. Adewunmi, R.M. Schek, C.L. Flanagan, P.H. Krebsbach, S.E. Feinberg, S.J. Hollister, S. Das, Biomaterials **26**, 4817 (2005)
S. Wust, R. Muller, S. Hofmann, J Funct Biomater **2**, 119 (2011)
X. Yan, D. Sun, IEEE Trans. Control Syst. Technol. **23**, 176 (2015)
M.G. Yeo, C.G. Simon, G.H. Kim, J. Mater. Chem. **22**, 21636 (2012)
Y.T. Zhang, F. Bottausci, M.P. Rao, E.R. Parker, I. Mezic, N.C. MacDonald, Biomed. Microdevices **10**, 509 (2008)
H. Zou, S. Mellon, R.R.A. Syms, K.E. Tanner, Biomed. Microdevices **8**, 353 (2006)